



OPEN An in-depth study of indolone derivatives as potential lung cancer treatment

Mohammed Er-rajy^{1,5}✉, Mohamed El fadili¹, Radwan Alnajjar², Sara Zarougui¹, Somdukt Mujwar³, Khalil Azzaoui^{4,5}, Hatem A. Abuelizz⁶, Belkheir Hammouti^{5,7} & Menana Elhallaoui¹

Lung cancer is a type of cancer that begins in the lungs and is one of the leading causes of cancer-related deaths worldwide. Herein an attempt to explore the relationship between the properties of indolone derivatives and their anticancer activity was investigated, implementing *in silico* approaches. Four indolone derivatives with the highest anticancer potential were selected to evaluate their pharmacological properties. The ADMET analysis revealed that these compounds exhibited favourable drug-like properties, meeting nearly all the key pharmacological criteria required for potential therapeutic agents. Molecular docking studies of the most active compounds revealed strong interactions with critical amino acid residues in the PDK1 receptor's binding site, underscoring their potential as effective PDK1 inhibitors. In addition, 200 ns molecular dynamics (MD) simulations of two R and S configurations validated the stability of the ligand-receptor complexes, with minimal structural deviations observed throughout the simulation period. These comprehensive results highlight the potential of the selected indolone derivatives as viable drug candidates and provide a solid foundation for future optimization efforts aimed at developing novel PDK1 inhibitors for cancer therapy.

Keywords PI3K-PDK1-AKT pathway, DFT study, Molecular docking, Molecular dynamic, ADMET properties

Cancer comprises a diverse group of diseases marked by the relentless and unregulated growth, proliferation, and division of cells¹. This unchecked cellular activity disrupts normal tissue function, often leading to the formation of malignant tumors and the potential spread of these abnormal cells to other parts of the body through a process known as metastasis². Such unrestrained cellular behavior is a fundamental hallmark of cancer, posing significant challenges to health and often necessitating complex therapeutic approaches. Once a cell undergoes malignant transformation, it can develop into various types of cancer. Lung cancer, in particular, is especially lethal due to its tendency to remain asymptomatic during the early stages³. In 2022, lung cancer was the leading cause of cancer-related mortality, responsible for 1.8 million deaths (18.7% of total cancer deaths) and approximately 2.5 million new cases annually, accounting for 12.4% of all new cancer diagnoses⁴. These sobering figures underscore the critical need for the development of novel chemotherapeutic agents, as the current arsenal of effective anticancer drugs remains limited. Additionally, the emergence of drug resistance further complicates treatment, highlighting the urgent demand for innovative therapeutic approaches to tackle this challenging disease.

Numerous signaling pathways are involved in the regulation of tumor processes, including the Wnt/ β -catenin, MAPK-RAS-RAF, VEGF, RTK, c-Met, NF κ B, RAF-MEK-ERK, and PI3K/AKT pathways, among others⁵⁻¹⁰. Each of these pathways plays a crucial role in specific mechanisms related to cancer cell proliferation, survival, and migration. We chose to focus on the PI3K-PDK1-AKT pathway due to its recent application in biomedical

¹LIMAS Laboratory, Faculty of Sciences Dhar El Mahraz, Sidi Mohamed Ben Abdellah University, Fez, Morocco.

²Department of Chemistry, Faculty of Science, University of Benghazi, Benghazi, Libya. ³Chitkara College of Pharmacy, Chitkara University, Rajpura, Punjab 140401, India. ⁴Engineering Laboratory of Organometallic,

Molecular Materials and Environment, Faculty of Sciences, Sidi Mohammed Ben Abdellah University, 30000 Fez, Morocco. ⁵Euromed University of Fes, UMF, 30000 Fes, Morocco. ⁶Department of Pharmaceutical Chemistry, College of Pharmacy, King Saud University, PO Box 2457, Riyadh 11451, Saudi Arabia.

⁷Laboratory of Industrial Engineering, Energy and the Environment (LI3E) SUPMTI, Rabat, Morocco. ✉email: mohammed.errajy@usmba.ac.ma

research and the promising results it has shown in the development of anticancer inhibitors, particularly for lung cancer treatment¹¹.

The PI3K-PDK1-AKT signaling pathway is crucial for regulating tumor proliferation, metastasis, invasion, and differentiation¹². This pathway is frequently overactivated in various cancers, making it a pivotal target in anticancer drug development¹³. Among the key proteins in this pathway, 3-phosphoinositide-dependent kinase-1 (PDK1) stands out as an essential kinase, often overexpressed in multiple cancers, and is thus a prime target for therapeutic intervention¹⁴. Molecular docking studies provide valuable insights into how potential drug molecules interact with their target proteins, aiding in the rational design of inhibitors¹⁵. Significant efforts are underway to identify potent PDK1 inhibitors by exploring diverse molecular scaffolds¹⁶.

Given the substantial time and resources required for drug discovery, computer-aided approaches such as ADMET propriety and molecular docking have become indispensable tools for optimizing the drug design process^{17–19}.

The discovery of new drug candidates is a lengthy and complex process, largely due to the limited number of effective anticancer agents and the emergence of resistance mechanisms^{20,21}. In response, major pharmaceutical companies are placing greater emphasis on innovation, incorporating advanced research methodologies to enhance the development pipeline, including predicting molecular activities before synthesis²². Molecular modeling techniques such as DFT, molecular docking, molecular dynamics, and ADMET analysis are invaluable tools for identifying and predicting promising drug candidates^{23–25}.

Materials and methods

Data set of molecules and calculation of the descriptors

An indolone dataset was collected in the literature²⁶. The molecular structures of the molecules studied, as well as their activity, are presented in Table S1.

ADMET prediction and DFT study

Drug similarity can be defined as a qualitative term used in drug design to assess the degree to which a substance is considered 'drug-like' compared to other compounds. When estimating the drug similarity of the design compounds (29, 35, 38, and 40), it is necessary to consider the alignment of the compound's physical and chemical properties with the filter criteria in order to calculate these properties for the four selected compounds.

Theoretical evaluations of all computational models were performed using the Gaussian 09 software²⁷, while the molecular structures were visualized with Gauss View 6.0.16. The geometric parameters for all configurations were determined using the DFT method with the B3LYP functional and the 6-31G basis set, ensuring accurate and reliable calculations for each system studied^{28–30}.

Molecular docking modeling

The two most active molecules were drawn in ChemDraw 16.0, and then the geometry was MM2 optimized^{31,32}. Both compounds were tested for their anti-lung activity. For the anti-lung study, we utilized the PDK1 receptor extracted from the Protein Data Bank (PDB ID: 1H1W)³³. A grid was created with parameters X = 42.550 Å, Y = 19.600 Å and Z = 3.000 Å.

For the molecular docking studies, we used the AutoDockTools software³⁴. A 60 × 60 × 60 grid was employed in the x, y, and z directions, with 200 solutions calculated for each case using a population size of 350. After meticulously preparing the molecules under study and their complexes, including the removal of water molecules, we proceeded with the molecular docking protocol to simulate potential interactions³⁵. Finally, to refine the analysis of ligand-protein interactions, we utilized Discovery 2021 software³⁶, which enabled not only the removal of residual water molecules but also the curation of incomplete side-chain residues and the optimization of structures by merging non-polar hydrogens, thereby enhancing the accuracy of the results obtained.

Molecular dynamic

Based on the molecular docking results, the two docked ligands were selected for MD simulations to verify the stability of their interactions with the target protein. MD simulations were performed using the Desmond program and Maestro from the Schrödinger Suite for 100 ns, employing the OPLS3e force field³⁷. The system was solvated in a 10 Å-sized aqueous box³⁸, and crystallographic water molecules were included using the single-point charge model under orthorhombic periodic boundary conditions³⁹.

The MD simulations were conducted under the NPT ensemble, using the Nosé-Hoover thermostat to maintain constant pressure (1 bar) and temperature (300 K)^{40,41}. The interaction diagram module of the Desmond simulation package was employed to analyze the specific binding interactions between the ligand and the protein⁴².

Results and discussion

Pharmaceutical properties

Four most active molecules were selected to evaluate their properties based on Lipinski's parameters; the results of the four most active molecule properties are presented in Table 1.

As shown in Table 1, the log P value of compound 35 exceeds the critical threshold of 5, indicating that while the other three compounds exhibit acceptable solubility in both aqueous and lipid environments, compound 35 is not soluble. The other parameters, such as topological polar surface area (TPSA) and the number of rotatable bonds (n-Rot), which are key bioavailability criteria, are also verified. Therefore, all of Lipinski's rules are met

Compounds	Property						Lipinski's violations	Synthetic accessibility
	MW	HBA	HBD	<i>n</i> -Rot	TPSA	LogP		
Threshold	< 500	< 10	< 5	≤ 10	≤ 140	≤ 5	≤ 1	
29	344.84	3	3	6	61.36	4.80	Yes	3.20
35	378.39	3	3	6	61.36	5.16	Yes	3.35
38	398.38	3	3	4	61.36	4.83	Yes	3.30
40	364.83	3	3	4	61.36	4.46	Yes	3.18

Table 1. Lipinski's role in the selection of four inhibitors. *MW* molecular weight, *HBA* H-bonds acceptors, *HBD* H-bonds donor, *n*-Rot number of rotatable bonds, *TPSA* topological polar surface area, *LogP* logarithm of the partition coefficient.

ID	Absorption	Distribution			Metabolism					Excretion	Toxicity	
		Intestinal absorption (human)	VDss (human)	BBB permeability	CNS permeability	Substrate		Inhibitor				
						CYP						
						2D6	3A4	1A2	2C19			2C9
Numeric (% Absorbed)	Numeric (Log L/kg)	Numeric (Log BB)	Numeric (Log PS)	Categorical (Yes/No)					Numeric (Log ml/min/kg)	Categorical (Yes/No)		
29	89.97	0.41	-0.078	-2.074	No	Yes	No	Yes	Yes	-0.335	No	
38	88.94	-0.15	-0.08	-1.78	No	Yes	Yes	Yes	Yes	-0.067	Yes	
40	90.6	-0.161	-0.086	-1.833	No	Yes	Yes	Yes	Yes	-0.132	Yes	

Table 2. ADMET prediction of selected molecules.

for compounds 29, 38, and 40, demonstrating that these three compounds have pharmaceutical properties comparable to those of reference anticancer drugs.

The three compounds underwent ADMET property prediction following the drug-likeness evaluation.

Following the drug similarity study, the three compounds were subjected to ADMET predictions. The pharmacokinetic properties (absorption, distribution, metabolism, excretion) and pharmacodynamic properties (drug efficacy and toxicity) are detailed in Table 2. The results indicate that all three compounds exhibit significant absorbance, suggesting good absorption in the human intestine. The volume of distribution (VDss) for compound 29 is considered high. Additionally, the blood-brain barrier (BBB) permeability values for all compounds fall within the acceptable range. For the central nervous system (CNS), values between -2 and -3 ⁴³ are expected, with compounds 30 and 40 falling outside the CNS threshold, whereas compound 29 shows the greatest potential for crossing the barrier.

All three compounds tested failed to inhibit the substrate of cytochrome P450 subtype 2D6⁴⁴. Compound 29 was also unable to inhibit the 1A2 enzyme. However, all three compounds were able to inhibit enzymes of cytochrome P450 subtypes 2C19, 3A4, and 2C9. All four compounds tested were substrates for cytochrome P450 enzymes.

In terms of excretion, the three compounds exhibited low total clearance values, indicating limited elimination. Furthermore, they were not identified as substrates of the organic cation transporter, a key transporter involved in renal absorption. This transporter plays a critical role in regulating the elimination and renal clearance of drugs and endogenous compounds, thereby contributing to the overall pharmacokinetics of these substances⁴⁵.

In terms of toxicity, which is crucial in drug selection, compound 29 is deemed non-toxic. In conclusion, ADMET analysis indicates that compound 29 has favorable pharmacokinetic properties.

The comprehensive ADMET profile of compound 29 highlights its potential to be developed into a safe, effective, and patient-friendly therapeutic option for lung cancer. Its remarkable combination of high oral bioavailability, targeted tissue distribution, metabolic stability, and minimal toxicity ensures sustained therapeutic efficacy while reducing the risk of adverse effects. These favorable pharmacokinetic and safety characteristics position compound 29 as a strong candidate for advancement into preclinical studies and subsequent clinical trials, paving the way for its potential clinical application in treating lung cancer.

Therefore, to understand the reactivity of this molecule, we conducted a DFT study with the B3LYP functional and the 6-31G basis set.

DFT analyses

Frontier molecular orbitals analysis (FMOs)

The FMO analysis is performed to assess the reactivity and characterize the nature of the excess electrons in the designed systems⁴⁶. Furthermore, the calculated energy values and the global descriptors are presented in Table 3.

As shown in Table 3, the HOMO and LUMO values were calculated to be -5.3592 eV and -1.0568 eV, respectively. The energy difference between HOMO and LUMO is thus 4.3023 eV, indicating a significant gap.

Parameters	Molecule N° 29
$E_{\text{LUMO}}/\text{eV}$	-1.0568
$E_{\text{HOMO}}/\text{eV}$	-5.3592
E_{gap}/eV	4.3023

Table 3. Chemical reactivity descriptors.

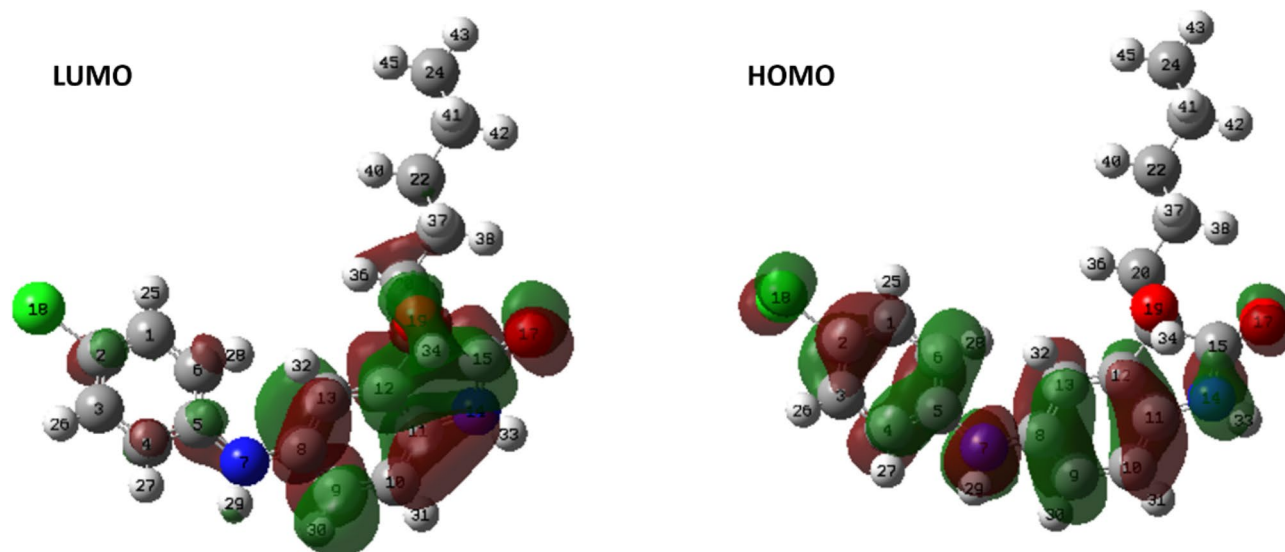


Fig. 1. The FMOs of studied molecules.

This E_{gap} suggests a potential charge transfer interaction within the studied molecule, indicating that the chosen molecule exhibits high chemical stability and low reactivity.

To better understand the distribution of electronic density for the HOMO and LUMO, we present the electronic density for each level in Fig. 1. This figure displays 3D plots or distributions of the HOMO and LUMO for the studied molecule.

As shown in Fig. 1, for the studied molecule, the HOMO orbital is located on the fragment 5-((4-chlorophenyl) amino)-3-hydroxyindolin-2-one, while the LUMO orbital is found on the group 3-hydroxyindolin-2-one. In other words, the group's 5-((4-chlorophenyl) amino)-3-hydroxyindolin-2-one and 3-hydroxyindolin-2-one act as electron donor and acceptor, respectively.

Molecular electrostatic potential analysis (MEP)

Using an electrostatic potential map to analyse the charge distribution and photophysical properties, it is possible to identify the regions subject to nucleophilic and electrophilic attack⁴⁷. Figure 2 displays the MEP diagrams for the studied molecule.

Based on the results achieved, the color range for the most active molecule goes from -6.275 e-2 to 6.275 e-2 , as shown in Fig. 2. In the molecule studied, it can be seen that there is only one region colored red located near the oxygen atom. This indicates that this atom is rich in electrons and therefore susceptible to electrophilic attack. On the other hand, there are two regions colored blue near the nitrogen atom. This indicates that this atom is electron-poor and therefore open to nucleophilic attack.

Molecular docking studies

To investigate molecular docking, we conducted an analysis of the two configurations of the most active molecule. Figure 3 presents the R and S configurations of this molecule.

The optimum result obtained, which is the lowest binding energy in kcal/mol for the molecules studied, is shown in Table 4.

For the R configuration, the optimum result obtained was the lowest binding energy of -4.743 kcal/mol . The molecular docking results for the R-configuration molecules examined are shown in Fig. 4.

Upon visual analysis of the results (Fig. 4), two hydrogen bonds are observed with the residues Lys-111, and Ala-162, with distances of 2.53 \AA and 2.89 \AA , respectively. Additionally, there are four alkyl and Pi-alkyl bonds with the residues Val-96, Leu-212, Ala-109, and Leu-88 with distances of 4.87 \AA , 4.69 \AA , 4.31 \AA , and 5.00 \AA , respectively. These results suggest that the molecule studied, compound No. 29 with R-configuration, could potentially serve as an effective inhibitor of the 1H1W receptor.

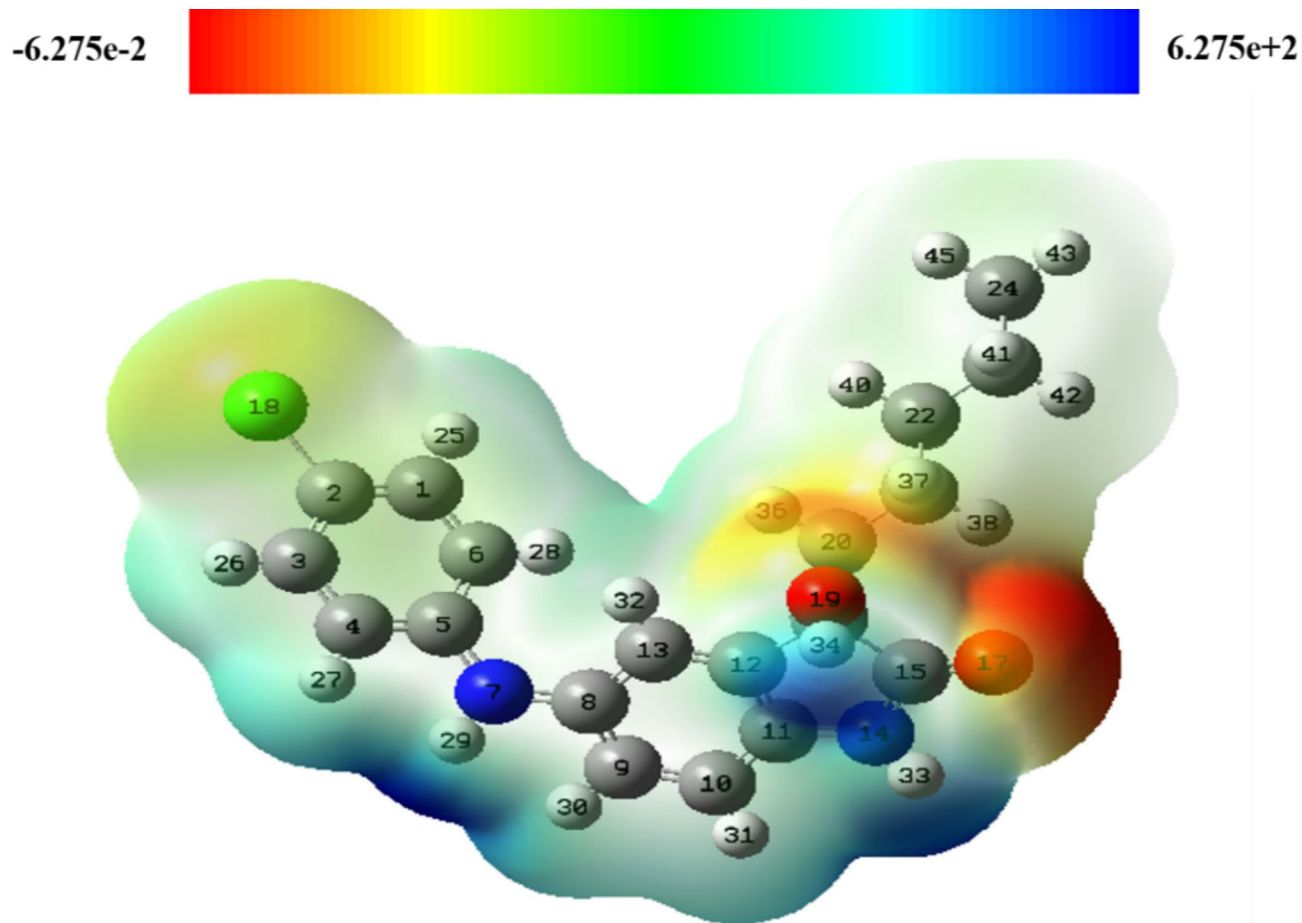


Fig. 2. Electrostatic potential maps (blue = electron-poor, red = electron-rich).

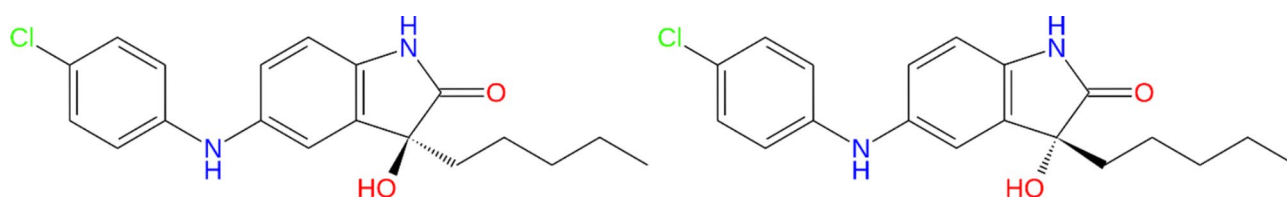


Fig. 3. Two possible configurations of molecules No. 29 R (left) and S (right).

For the S configuration, the optimum result obtained was the lowest binding energy of -5.026 kcal/mol. The molecular anchoring results for the S-configuration molecules examined are shown in Fig. 5.

Upon visual analysis of the results (Fig. 5), two hydrogen bonds are observed with the residues Lys-111 and Ala-162, with distances of 2.74 Å and 1.98 Å, respectively. Additionally, there are four alkyl and Pi-alkyl bonds with the residues Val-96, Leu-212, Ala-109, and Leu-88 with distances of 4.98 Å, 4.71 Å, 4.66 Å, and 4.25 Å, respectively. These results suggest that the molecule studied, compound No. 29 with S-configuration, could potentially serve as an effective inhibitor of the 1H1W receptor.

For the reference molecule, the optimum result obtained was the lowest binding energy of -10.053 kcal/mol. The molecular anchoring results for the reference molecule are shown in Fig. 6.

Upon visual analysis of the results (Fig. 6), eight hydrogen bonds are observed with the residues Ser-94, Ser-92, Phe-93, Gly-91, Ser-160, Ala-162, Leu-88, and Gly-166, with distances of 2.12 Å, 3.45 Å, 1.77 Å, 2.60 Å, 1.94 Å, 2.63 Å, 2.86 Å, and 1.69 Å, respectively. Additionally, there is one salt bridge and attractive charge bond with the residues Lys-111 at a distance of 2.63 Å and 2.23 Å. Lastly, the molecule establishes four Pi-alkyl bonds with the residues Ala-109, Ala-109, and Val-96. These interactions play a pivotal role in advancing key studies, underscoring the critical importance of these enzymes in the regulation of cancer cell proliferation^{48–50}. Their involvement is particularly significant in the context of lung cancer, where they contribute to understanding the molecular mechanisms underlying tumor growth and potential therapeutic interventions.

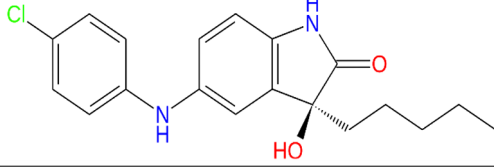
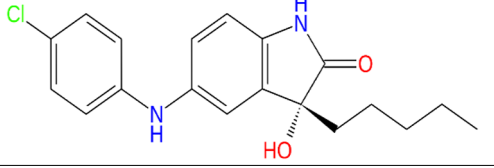
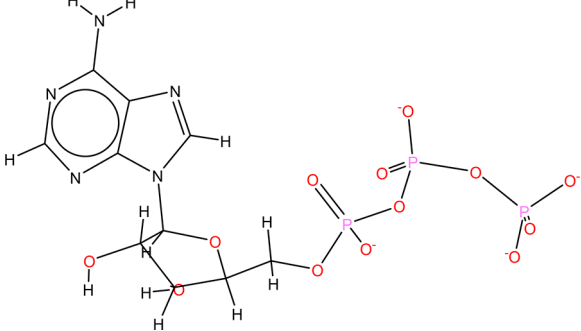
Ligand	Structural formula	Binding Energy (kcal/mol)	Binding residue
R-Configurations of M. No. 29		-4.743	Lys-111, Ala-162, Val-96, Leu-212, Ala-109 and Leu-88
S-Configurations of M. No. 29		-5.026	Lys-111, Ala-162, Val-96, Leu-212, Ala-109 and Leu-88.
Reference molecule studied of the receptor 1H1W		-10.053	Ser-94, Ser-92, Phe-93, Gly-91, Ser-160, Ala-162, Leu-88, Gly-166, Lys-111, Ala-109, Ala-109, and Val-96

Table 4. Docking results for compounds studied against potent PDK1 inhibitors (1H1W).

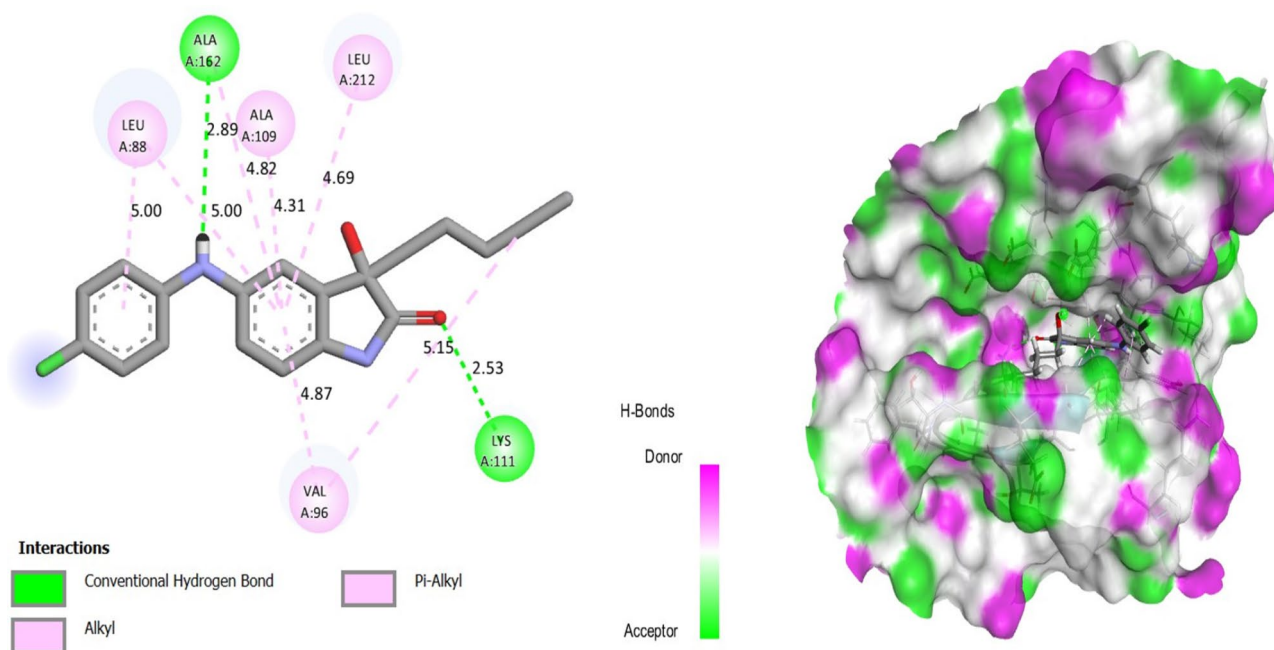


Fig. 4. The 2/3D interactions between the R-configuration molecule studied and the 1H1W receptor.

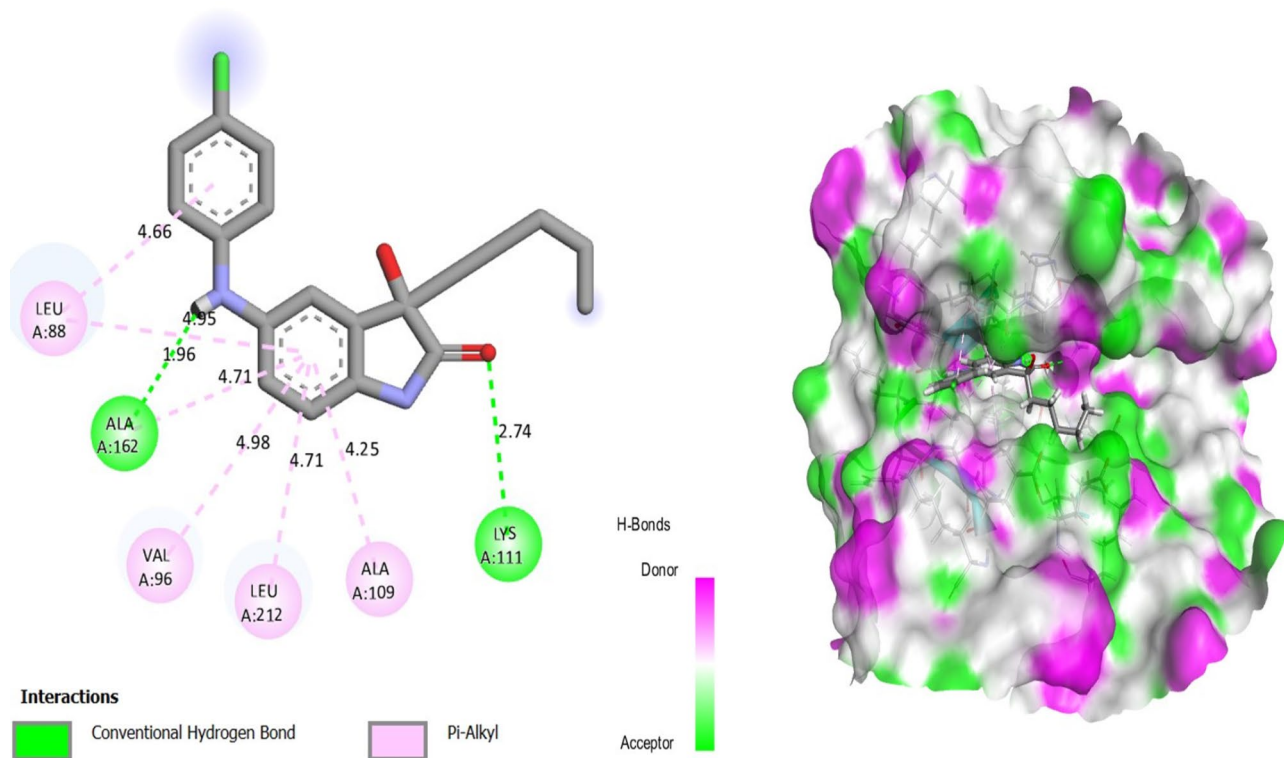


Fig. 5. The 2/3D interactions between the S-configuration molecule studied and the 1H1W receptor.

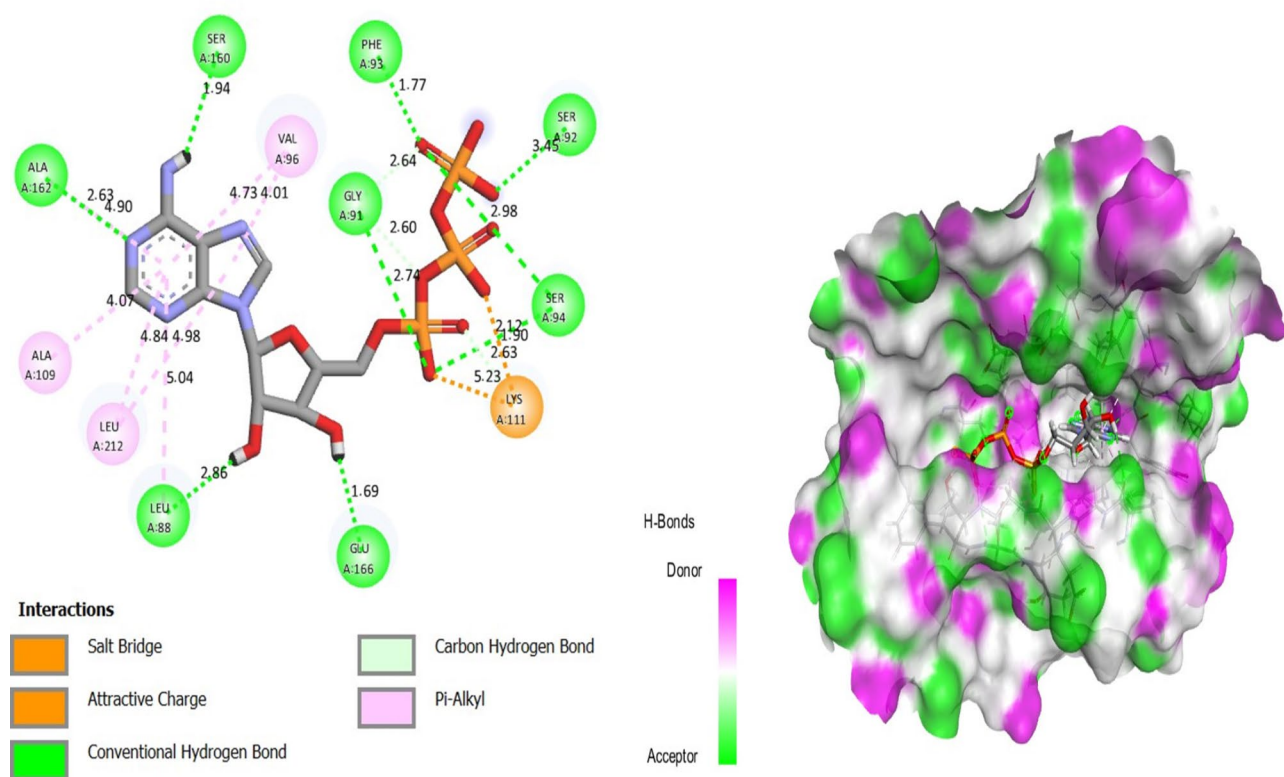


Fig. 6. The 2/3D interactions between the reference molecule studied and the receptor 1H1W.

These results suggest that the studied molecule targets almost the same residues as those bound to the reference molecule, confirming that the two selected inhibitors could serve as effective inhibitors of the 1H1W receptor.

Molecular dynamic

The interactions between the protein and the ligand, as indicated by the RMSD, RMSF, and interaction fraction parameters, were analyzed to assess the MD trajectories^{51,52}. MD modeling has proven to be an effective method for studying the stability of ligand docking poses and the roles of key amino acids in proteins. To assess the stability of the complexes and observe the potential binding modes of the ligands, we conducted 200 ns MD simulations on the selected molecule.

The RMSD (Root Mean Square Deviation)⁵³ value provides insights into the stability of the ligand-protein complex interactions (Fig. 7). In this case, the R-M29 molecule exhibits less stability compared to the S-M29 compound. However, R-M29 demonstrates good stability beginning at the 100 ns mark, with an RMSD of 4.8 Å, accompanied by some fluctuations that do not significantly affect the overall stability of the complex. Additionally, an RMSD value of 4.8 Å is generally considered acceptable for comparing the two different structures (ligand R-M29 and protein) at the atomic level. On the other hand, the S configuration molecule demonstrates greater stability compared to the R configuration. This molecule exhibits consistent stability over 100 ns, from 75 ns to 175 ns, maintaining a distance of 3.6 Å with no fluctuations. This indicates that the S-configuration experiences less deviation during the simulation between the two different structures (ligand S-M29 and protein) at the atomic level when compared to the R-configuration molecule. For the reference molecule, the average RMSD value of the complex (Reference molecule-1H1W) was approximately 3.2 Å over the 200 ns simulation. The molecule exhibited good stability, with a minor fluctuation decrease at 150 ns, dropping to 2.4 Å, which did not compromise the stability of the complex when comparing the three molecules. Notably, the molecule S-M29

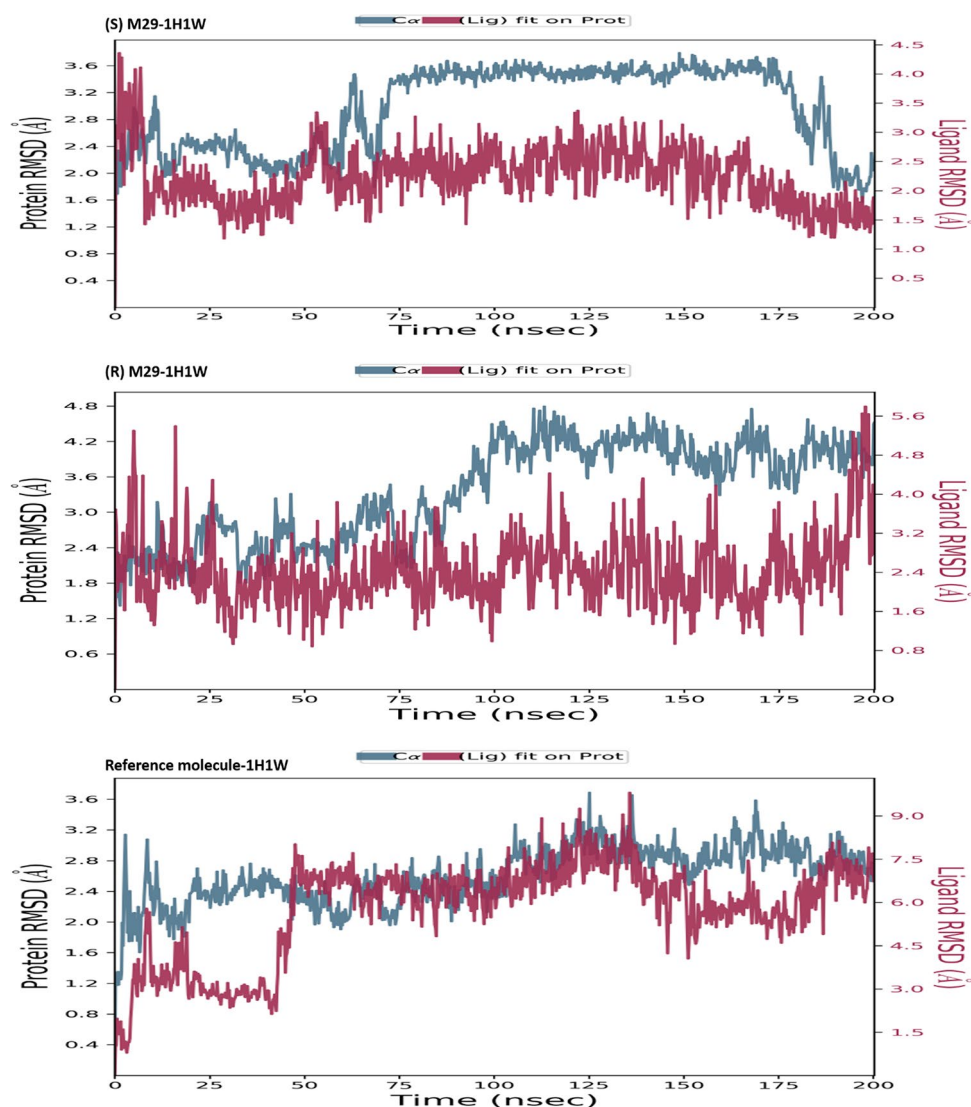


Fig. 7. RMSD of two complex configurations (R and S) M 29-1H1W and the reference molecule-1H1W.

demonstrated stability similar to that of the reference molecule. The analysis of the interactions obtained between the macromolecular complexes of the two configurations of the molecule M29 (R and S) and the reference molecule during a 200 ns MD simulation, illustrated in Fig. 8, shows that the macromolecular structure, which includes the amino acid LYS-111, exhibited a 70% hydrogen bond interaction and a 30% water bridge interaction. Additionally, the amino acid GLU-166 displays a 20% water bridge interaction in molecule S-M29. For the complex (R-M29, 1H1W), the macromolecular structure indicated that the amino acid LYS-111 exhibited 10% water bridge interactions, while the amino acid GLU-166 showed 70% hydrogen bond interactions and 30% water bridge interactions. On the other hand, the structure of the macromolecule (reference molecule 1H1W) indicated that the amino acid LYS-111 exhibited 10% hydrogen bond interactions, 5% ionic interactions, and 40% water bridge interactions, while the amino acid GLU-166 showed 20% hydrogen bond interactions, 40% ionic interactions, and 20% water bridge interactions.

Structural modifications in root mean square fluctuations (RMSF)⁵⁴ were also analyzed to evaluate the influence of the two configurations of the M29 molecule (R and S) binding to the target protein in order to compare these results with the RMSF findings for the reference molecule. The RMSF results illustrated in Fig. 9 indicate that only a limited number of insignificant fluctuations are above 3 Å, suggesting that all other fluctuations are in a reasonable range. Finally, the two configurations of the M29 molecule (R and S) demonstrate good stability during 200 ns of dynamic simulation when compared to the reference molecule binding to the target protein 1H1W; however, the R-M29 configuration exhibits greater stability.

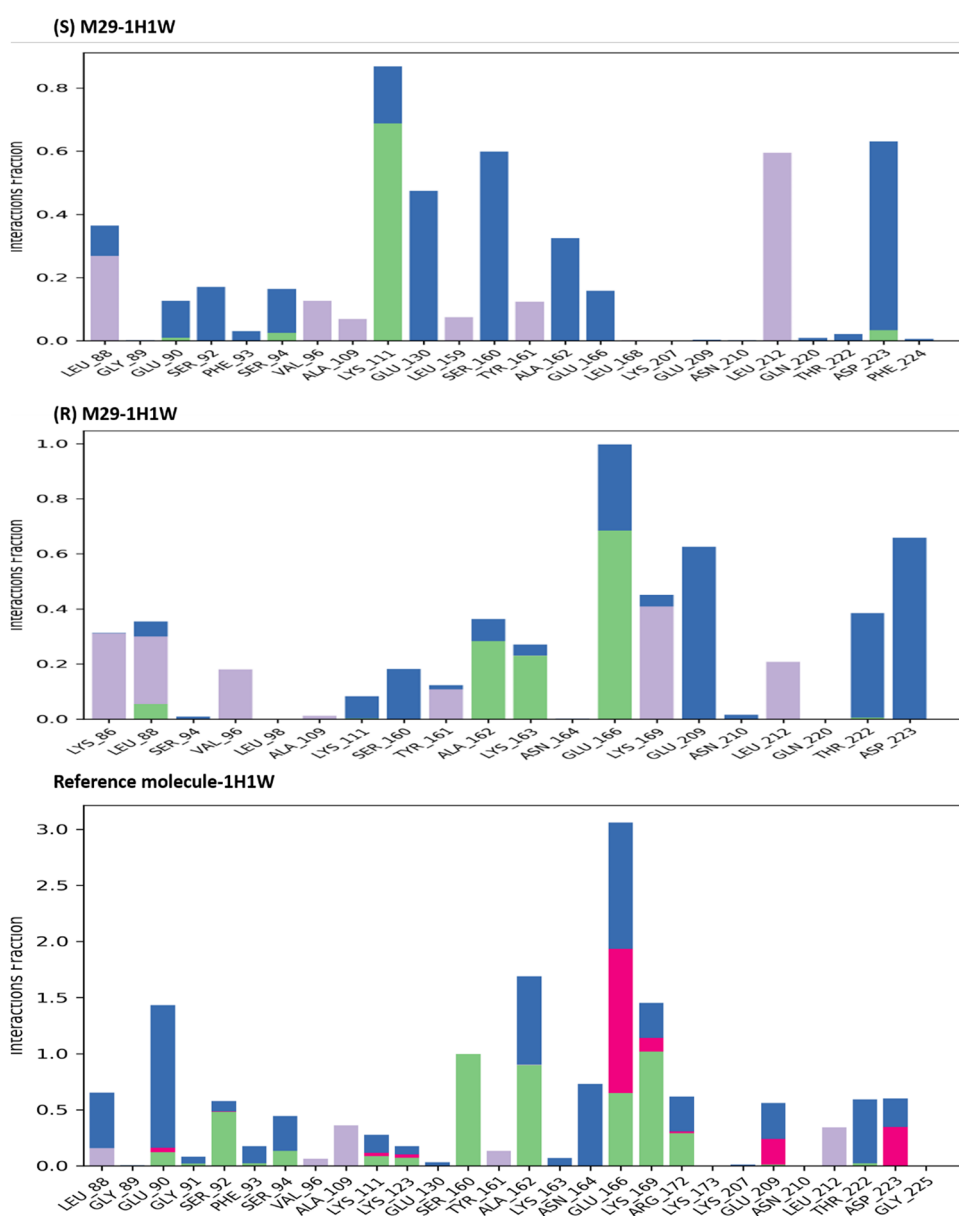


Fig. 8. Interaction fraction of two complex configurations (R and S) M29-1H1W and the reference molecule-1H1W.

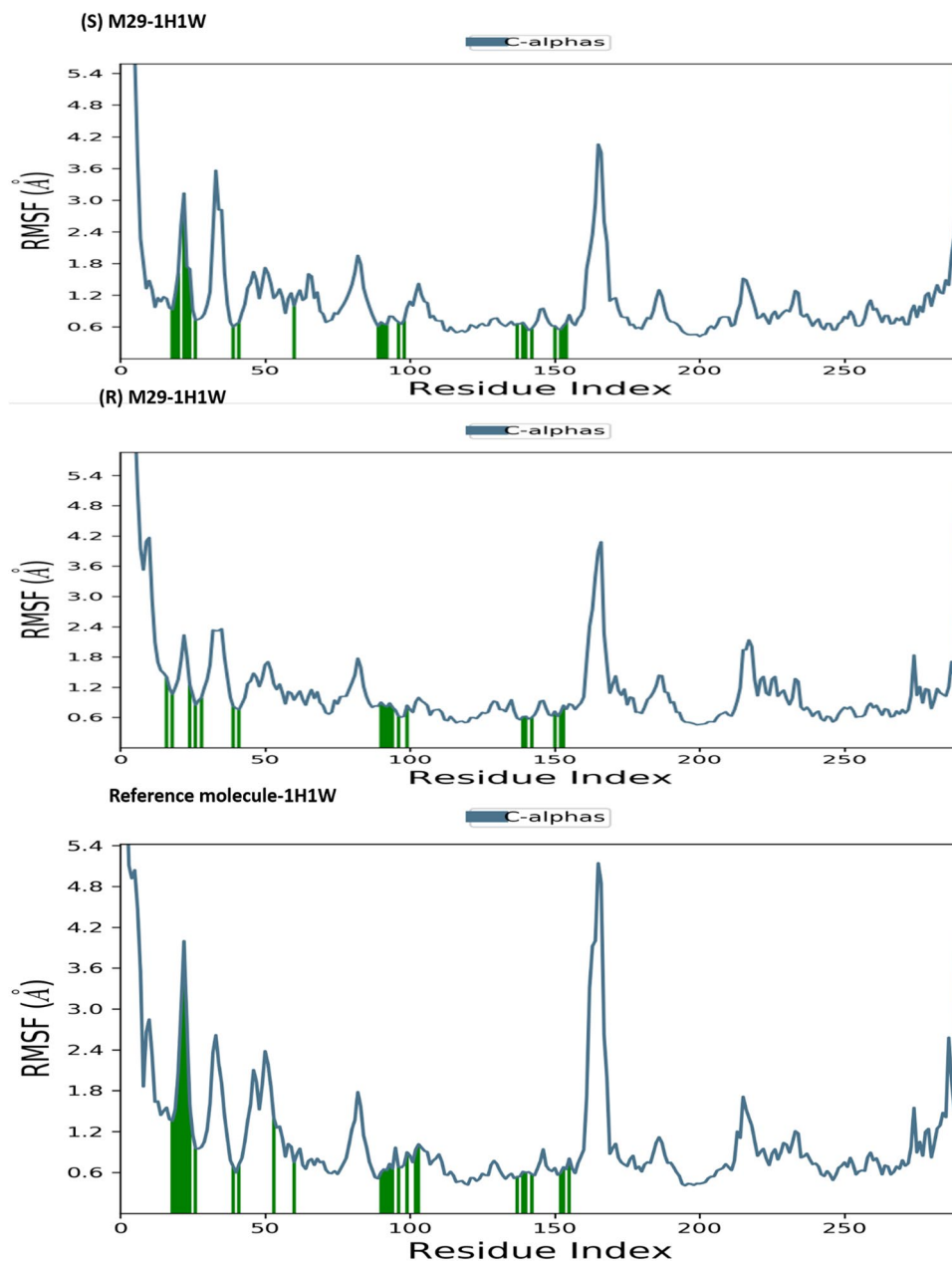


Fig. 9. RMSF of two complex configurations (R and S) M 29-1H1W and the reference molecule-1H1W.

Conclusion

To investigate and interpret the relationship between the properties of indolone derivatives and their anti-lung cancer activity, we carried out a theoretical molecular modeling study. We selected four indolone derivative molecules with the best anti-lung cancer activity in order to assess their drug-like properties. The results showed that molecule 29 had acceptable pharmacological properties, making it an excellent candidate for drug discovery. A reactivity study using DFT shows that this compound exhibits reactivity at the oxygen and nitrogen atoms, allowing it to react with other molecules or enzymes. This compound was analyzed through molecular docking studies, which revealed that its interactions with the kinase receptor 1W1H exhibit significant stability, primarily due to multiple hydrogen bonds. Furthermore, the selected molecule was optimally positioned within the binding cavity of the protein. To further assess the stability of the formed complex, molecular dynamics simulations were performed. The results demonstrated that the complex maintained remarkable stability over the 100 ns simulation period. Based on these findings, compound 29 can be proposed as a promising anti-cancer candidate for the treatment of lung cancer.

Data availability

<https://doi.org/10.1016/j.bmc.2019.01.028>.

Received: 12 November 2024; Accepted: 6 January 2025

Published online: 16 January 2025

References

1. Bisoyi, P. A brief tour guide to cancer disease. In *Understanding Cancer* (eds Jain, B. & Pandey, S.) 1–20 (Academic, 2022). <https://doi.org/10.1016/B978-0-323-99883-3.00006-8>.
2. Bhat, G. R. et al. Cancer cell plasticity: from cellular, molecular, and genetic mechanisms to tumor heterogeneity and drug resistance. *Cancer Metastasis Rev.* **43**, 197–228 (2024).
3. Petty, T. L. The early diagnosis of lung cancer. *Dis. Mon.* **47**, 197–264 (2001).
4. Kratzer, T. B. et al. Lung cancer statistics, 2023. *Cancer* **130**, 1330–1348 (2024).
5. Xia, L. et al. Role of the NF κ B-signaling pathway in cancer. *OncoTargets Ther.* **11**, 2063–2073 (2018).
6. Bartholomeusz, C. & Gonzalez-Angulo, A. M. Targeting the PI3K signaling pathway in cancer therapy. *Expert Opin. Ther. Targets.* **16**, 121–130 (2012).
7. Regad, T. Targeting RTK signaling pathways in cancer. *Cancers* **7**, 1758–1784 (2015).
8. Peruzzi, B. & Bottaro, D. P. Targeting the c-Met signaling pathway in cancer. *Clin. Cancer Res.* **12**, 3657–3660 (2006).
9. Stacker, S. A. & Achen, M. G. The VEGF signaling pathway in cancer: the road ahead. *Chin. J. Cancer.* **32**, 297–302 (2013).
10. Zhang, Y. & Wang, X. Targeting the Wnt/ β -catenin signaling pathway in cancer. *J. Hematol. Oncol. J. Hematol. Oncol.* **13**, 165 (2020).
11. Huang, K. et al. Naomaitai ameliorated brain damage in rats with vascular dementia by PI3K/PDK1/AKT signaling pathway. *Evid. Based Complement. Altern. Med.* **2019**, 2702068 (2019).
12. Carnero, A. The PKB / AKT pathway in Cancer 34–44 (2010).
13. Garcia-Echeverria, C. & Sellers, W. R. Drug discovery approaches targeting the PI3K/Akt pathway in cancer. *Oncogene* **27**, 5511–5526 (2008).
14. Stout, T., Foster, P. & Matthews, D. High-throughput structural biology in drug discovery: protein kinases. *Curr. Pharm. Des.* **10**, 1069–1082 (2005).
15. Er-rajiy, M. et al. 2D-QSAR modeling, drug-likeness studies, ADMET prediction, and molecular docking for anti-lung cancer activity of 3-substituted-5-(phenylamino) indolone derivatives. *Struct. Chem.* <https://doi.org/10.1007/s11224-022-01913-3> (2022).
16. Liu, R. et al. A novel PDK1/MEK dual inhibitor induces cytoprotective autophagy via the PDK1/Akt signaling pathway in non-small cell lung cancer. *Pharmaceuticals* **16**, 244 (2023).
17. Nordberg, J. & Arnér, E. S. J. Reactive oxygen species, antioxidants, and the mammalian thioredoxin system. *Free Radic Biol. Med.* **31**, 1287–1312 (2001).
18. Moussaoui, M. et al. QSAR, ADMET, molecular docking, and dynamics studies of 1,2,4-triazine-3(2H)-one derivatives as tubulin inhibitors for breast cancer therapy. *Sci. Rep.* **14**, 16418 (2024).
19. Huang, A. A. & Huang, S. Y. Increasing transparency in machine learning through bootstrap simulation and shapely additive explanations. *PLOS ONE.* **18**, e0281922 (2023).
20. Zarougui, S. et al. QSAR, DFT studies, docking molecular and simulation dynamic molecular of 2-styrylquinoline derivatives through their anticancer activity. *J. Saudi Chem. Soc.* **27**, 101728 (2023).
21. Huang, A. A. & Huang, S. Y. Computation of the distribution of model accuracy statistics in machine learning: comparison between analytically derived distributions and simulation-based methods. *Health Sci. Rep.* **6**, e1214 (2023).
22. Er-rajiy, M. et al. QSAR, molecular docking, and molecular dynamics simulation-based design of novel anti-cancer drugs targeting thioredoxin reductase enzyme. *Struct. Chem.* 1–17 (2023).
23. Er-rajiy, M. et al. Design of novel anti-cancer agents targeting COX-2 inhibitors based on computational studies. *Arab. J. Chem.* **105193** <https://doi.org/10.1016/j.arabjc.2023.105193> (2023).
24. Er-rajiy, M., Fadili, E., Mrabti, M., Zarougui, N. N., Elhallaoui, M. & S. & QSAR, molecular docking, ADMET properties in silico studies for a series of 7-propanamide benzoxaboroles as potent anti-cancer agents. *Chin. J. Anal. Chem.* **50**, 100163 (2022).
25. Moussaoui, M. et al. In silico design of novel CDK2 inhibitors through QSAR, ADMET, molecular docking and molecular dynamics simulation studies. *J. Biomol. Struct. Dyn.* **41**, 13646–13662 (2023).
26. Yu, Z. et al. Dual inhibitors of RAF-MEK-ERK and PI3K-PDK1-AKT pathways: design, synthesis and preliminary anticancer activity studies of 3-substituted-5-(phenylamino) indolone derivatives. *Bioorg. Med. Chem.* **27**, 944–954 (2019).
27. Tomberg, A. Gaussian 09w Tutorial an introduction to Computational Chemistry using G09w and Avogadro Software.–2020. *There no Corresp. Rec. this Ref.* 1–36 (2021).
28. Edder, Y. et al. Synthesis of novel nitro-halogenated aryl-himachalene sesquiterpenes from atlas cedar oil components: characterization, DFT studies, and Molecular Docking Analysis against various isolated smooth muscles. *Molecules* **29**, 2894 (2024).
29. Zarougui, S. et al. 3D computer modeling of inhibitors targeting the MCF-7 breast cancer cell line. *Front. Chem.* **12**, 1384832 (2024).
30. van Mourik, T., Bühl, M. & Gaigeot, M. P. Density functional theory across chemistry, physics and biology. *Philos. Trans. R Soc. Math. Phys. Eng. Sci.* **372**, 20120488 (2014).
31. Aloui, M. et al. QSAR modelling, molecular docking, molecular dynamic and ADMET prediction of pyrrolopyrimidine derivatives as novel Bruton's tyrosine kinase (BTK) inhibitors. *Saudi Pharm. J.* **32**, 101911 (2024).
32. Er-Rajy, M., Faris, A., Zarougui, S. & Elhallaoui, M. Design of potential anti-cancer agents as COX-2 inhibitors, using 3D-QSAR modeling, molecular docking, oral bioavailability proprieties, and molecular dynamics simulation. *Anticancer Drugs* **35**, 117–128 (2024).
33. Iams, V. et al. Mechanism of the Orotidine 5'-Monophosphate decarboxylase-catalyzed reaction: importance of residues in the Orotate binding site. *Biochemistry* **50**, 8497–8507 (2011).
34. Holt, P. A., Chaires, J. B. & Trent, J. O. Molecular docking of intercalators and groove-binders to nucleic acids using autodock and Surflex. *J. Chem. Inf. Model.* **48**, 1602–1615 (2008).
35. Abdul Amin, S., Adhikari, N., Agrawal, K., Jha, R. & Gayen, S. Possible binding mode analysis of pyrazolo-triazole hybrids as potential anticancer agents through validated molecular docking and 3D-QSAR modeling approaches. *Lett. Drug Des. Discov.* **14**, 515–527 (2017).
36. Molecular Docking. Shifting paradigms in drug discovery. <https://www.mdpi.com/1422-0067/20/18/4331>
37. Roos, K. et al. OPLS3e: extending force field coverage for drug-like small molecules. *J. Chem. Theory Comput.* **15**, 1863–1874 (2019).
38. Kurki, M., Poso, A., Bartos, P. & Miettinen, M. S. Structure of POPC lipid bilayers in OPLS3e force field. *J. Chem. Inf. Model.* **62**, 6462–6474 (2022).
39. Boily, J. F. The variable capacitance model: a strategy for treating contrasting charge-neutralizing capabilities of counterions at the Mineral/Water Interface. *Langmuir* **30**, 2009–2018 (2014).
40. Schulz, R., Lindner, B., Petridis, L. & Smith, J. C. Scaling of multimillion-atom biological molecular dynamics simulation on a petascale supercomputer. *J. Chem. Theory Comput.* **5**, 2798–2808 (2009).
41. Ke, Q., Gong, X., Liao, S., Duan, C. & Li, L. Effects of thermostats/barostats on physical properties of liquids by molecular dynamics simulations. *J. Mol. Liq.* **365**, 120116 (2022).

42. Scarabelli, G., Oloo, E. O., Maier, J. K. X. & Rodriguez-Granillo, A. Accurate prediction of protein thermodynamic stability changes upon residue mutation using free energy perturbation. *J. Mol. Biol.* **434**, 167375 (2022).
43. O'Connor, J. et al. Orthotic management of instability of the knee related to neuromuscular and central nervous system disorders: systematic review, qualitative study, survey and costing analysis. *Health Technol. Assess. Winch. Engl.* **20**, 1–262 (2016).
44. Nebert, D. W. & Russell, D. W. Clinical importance of the cytochromes P450. *Lancet* **360**, 1155–1162 (2002).
45. da Silva, D. V. S. P. et al. In vitro activity, ultrastructural analysis and *in silico* pharmacokinetic properties (ADMET) of thiazole compounds against adult worms of *Schistosoma mansoni*. *Acta Trop.* **245**, 106965 (2023).
46. Zhang, J. & Cashman, J. R., Quantitative analysis of FMO gene mRNA levels in human tissues. *Drug Metab. Dispos.* **34**, 19–26 (2006).
47. Er-rajy, M. et al. 3D-QSAR studies, molecular docking, molecular dynamic simulation, and ADMET proprieties of Novel pteridinone derivatives as PLK1 inhibitors for the treatment of prostate Cancer. *Life* **13**, 127 (2023).
48. Barile, E., De, S. K. & Pellicchia, M. PDK1 inhibitors. *Pharm. Pat. Anal.* **1**, 145–163 (2012).
49. Goldsmith, E. J., Akella, R., Min, X., Zhou, T. & Humphreys, J. M. Substrate and docking interactions in Serine/Threonine protein kinases. *Chem. Rev.* **107**, 5065–5081 (2007).
50. Kirubakaran, P., Muthusamy, K., Singh, K. H. D. & Nagamani, S. Ligand-based Pharmacophore Modeling; atom-based 3D-QSAR analysis and molecular Docking studies of Phosphoinositide-Dependent Kinase-1 inhibitors. *Indian J. Pharm. Sci.* **74**, 141–151 (2012).
51. Er-Rajy, M., Fadili, E., Mujwar, M., Zarougui, S., Elhallaoui, M. & S. & Design of novel anti-cancer drugs targeting TRKs inhibitors based 3D QSAR, molecular docking and molecular dynamics simulation. *J. Biomol. Struct. Dyn.* <https://doi.org/10.1080/07391102.2023.2170471> (2023).
52. da Fonseca, A. M. et al. Screening of potential inhibitors targeting the main protease structure of SARS-CoV-2 via Molecular Docking, and Approach with Molecular Dynamics, RMSD, RMSF, H-Bond, SASA and MMGBSA. *Mol. Biotechnol.* **66**, 1919–1933 (2024).
53. Dixit, S. B., Ponomarev, S. Y. & Beveridge, D. L. Root mean square deviation probability analysis of molecular dynamics trajectories on DNA. *J. Chem. Inf. Model.* **46**, 1084–1093 (2006).
54. Keskin, O., Jernigan, R. L. & Bahar, I. Proteins with similar architecture exhibit similar large-scale dynamic behavior. *Biophys. J.* **78**, 2093–2106 (2000).

Acknowledgements

The authors extend their appreciation to the Researchers Supporting Project, King Saud University, Riyadh, Saudi Arabia for funding this work through grant number RSPD2025R566.

Author contributions

Author contributions; Mohammed Er-rajy: Data curation, Formal analysis, Methodology, Resources, Software, Writing - original draft, Writing - review editing. Mohamed El Fadili: Supervision, Visualization. Radwan Al-najjar : Supervision, Visualization, MD simulation. Sara Zarougui: Supervision, Visualization. Somdutt Mujwar : Supervision, Visualization, MD simulation. Khalil Azzouai: Supervision, Visualization. Hatem A. Abuelizz: Supervision, Validation. Belkheir Hammouti: Supervision, Visualization. Menana Elhallaoui: Conceptualization, Methodology, Project administration, Supervision, Validation, Visualization, Writing - review & editing.

Funding

This research was funded by the Researchers Supporting Project (number RSPD2024R566), King Saud University, Riyadh, Saudi Arabia.

Declarations

Competing interests

The authors declare no competing interests.

Additional information

Supplementary Information The online version contains supplementary material available at <https://doi.org/10.1038/s41598-025-85707-7>.

Correspondence and requests for materials should be addressed to M.E.-r.

Reprints and permissions information is available at www.nature.com/reprints.

Publisher's note Springer Nature remains neutral with regard to jurisdictional claims in published maps and institutional affiliations.

Open Access This article is licensed under a Creative Commons Attribution-NonCommercial-NoDerivatives 4.0 International License, which permits any non-commercial use, sharing, distribution and reproduction in any medium or format, as long as you give appropriate credit to the original author(s) and the source, provide a link to the Creative Commons licence, and indicate if you modified the licensed material. You do not have permission under this licence to share adapted material derived from this article or parts of it. The images or other third party material in this article are included in the article's Creative Commons licence, unless indicated otherwise in a credit line to the material. If material is not included in the article's Creative Commons licence and your intended use is not permitted by statutory regulation or exceeds the permitted use, you will need to obtain permission directly from the copyright holder. To view a copy of this licence, visit <http://creativecommons.org/licenses/by-nc-nd/4.0/>.

© The Author(s) 2025